Fully Nonorthogonal Higher-Order FDTD Schemes for the Systematic Development of 3-D PML's in General Curvilinear Coordinates

Nikolaos V. Kantartzis, *Student Member, IEEE*, Theodoros I. Kosmanis, *Student Member, IEEE*, and Theodoros D. Tsiboukis, *Senior Member, IEEE*

***Abstract*—The efficient construction of reflectionless PML's in 3-D curvilinear coordinates via a new higher-order FDTD methodology, is presented in this paper. By accurately treating the div-curl problem, the technique introduces a higher-order rendition of the covariant/contravariant vector theory with generalized conventional and nonstandard schemes. Moreover, a mesh expansion algorithm decreases the absorbers' thickness. In the time domain, the four-stage Runge–Kutta integrator is also invoked, while the wider spatial stencils are effectively limited by self-adaptive compact operators. Numerical verification indicates that the novel PML's offer a serious suppression of dispersion errors and significant savings in the computational burden.**

***Index Terms*—Curvilinear nonorthogonal coordinates, FDTD methods, higher-order schemes, perfectly matched layers.**

I. Introduction

THE CONSISTENT modeling of arbitrarily curved geometries in general curvilinear coordinates, via body-conformed FDTD mapping and the constantly developing perfectly matched layer (PML) [1]–[5], is being intensively investigated [6]. Lately, various efficient methods extended the versatility of the absorber to curvilinear grids. In [7], [8] split-field PML's are derived, while [9] introduces an unsplit medium involving nonorthogonal discretization. The application of uniaxial PML's to conformal FDTD meshes is investigated in [10] and in [11], a Maxwellian well-posed sponge layer, for the three coordinate systems, is thoroughly presented.

It is the objective of this paper to introduce a novel fully nonorthogonal higher-order FDTD technique—founded on advanced conventional and nonstandard concepts—for the construction of 3-D curvilinear PML's. Its essential premise is field representation via a modified higher-order covariant and contravariant strategy (Fig. 1) that stems from an efficient solution of the strenuous div-curl problem on an unstructured mesh. Apart from the leapfrog process, the Runge–Kutta operators are alternatively utilized, while new self-adaptive compact operators treat the widened spatial stencils. Hence, reduced dispersion and lattice reflection errors are obtained and the grid more easily copes with the rapidly increasing PML losses. To achieve improved attenuation, the layers are backed by lossy absorbing boundary conditions (ABC's). Furthermore, a curvilinear mesh expansion approach provides larger cell sizes for a specific accuracy level. Numerical evaluation examines PML behavior as a function of distance from the scatterer, the convergence properties with respect to lattice resolution and the evolution of different error norms.

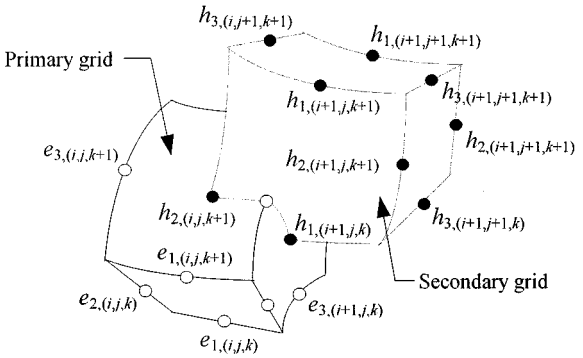

Fig. 1. A nonorthogonal curvilinear lattice with its covariant components.

II. Higher-Order Nonorthogonal FDTD Schemes

The primary attribute of the new FDTD methodology are the higher-order nonstandard concepts, which approximate the spatial and temporal derivatives. Therefore, we introduce

$$\boldsymbol{DS}_u^{nst}[f] = \frac{11}{12}\boldsymbol{D}_{u,\,\delta u}^{nst}[f] + \frac{1}{24\delta u} \cdot \left(\delta u \boldsymbol{D}_{u,\,3\delta u}^{nst}[f] + f\big|_{u-(\delta u/2)}^{t} - f\big|_{u-(3u/2)}^{t}\right),$$

where u is a variable of the general coordinate system $(u,\, v,\, w)$ and $\boldsymbol{D}_{u,\,\delta h}^{nst}[.]$ $(\delta h = \delta u,\, 3\delta u)$ the 3-D nonstandard operator

$$\boldsymbol{D}_{u,\,\delta h}^{nst}[f] \equiv \frac{1}{m_k(\delta h)}\left(q_1 \boldsymbol{d}_{u,\,\delta h}^{(1)}[f] + q_2 \boldsymbol{d}_{u,\,\delta h}^{(2)}[f] + q_3 \boldsymbol{d}_{u,\,\delta h}^{(3)}[f]\right). \quad (1)$$

The correction function $m_k(\delta h)$ in (1), minimizes derivative approximation errors and significantly improves dispersion and dissipation characteristics. A possible selection could be

$$m_k(\delta h) = \frac{5}{k}\cos\left(\frac{k\delta h}{4}\right) \qquad \text{such that}$$
$$\boldsymbol{D}_{u,\,\delta h}^{nst} e^{jku} = \partial_u (e^{jku}),$$

Manuscript received October 25, 1999.

The authors are with the Department of Electrical and Computer Engineering, Aristotle University of Thessaloniki, Thessaloniki, GR 54006 Greece (e-mail: tsibukis@eng.auth.gr).

Publisher Item Identifier S 0018-9464(00)05361-9.

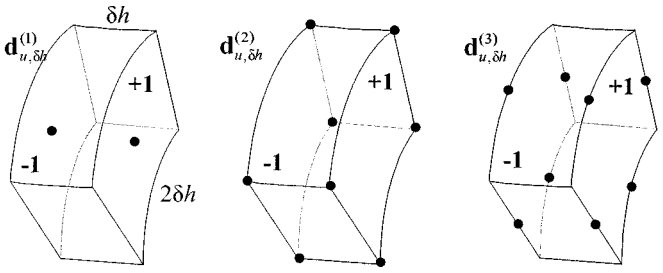

Fig. 2. Graphical depiction of the curvilinear finite-difference operators. The numbers at the faces indicate the sign of summation in the expressions.

is fulfilled with $\boldsymbol{k}$ denoting the wave number. To perform a highly accurate transition to the discretized space, $\boldsymbol{d}$ operators for $p = 1, 2, 3$, are cast on the following form which completely exploits the geometry of the elementary cell, as in Fig. 2

$$\boldsymbol{d}^{(1)}_{u,\delta h}[f] = f|^t_{\delta h/2,0,0} - f|^t_{-\delta h/2,0,0}, \tag{2}$$

$$\boldsymbol{d}^{(2)}_{u,\delta h}[f] = \frac{1}{2}\begin{pmatrix} f|^t_{\delta h/2,\delta h,\delta h} + f|^t_{\delta h/2,\delta h,-\delta h} + f|^t_{\delta h/2,-\delta h,\delta h} \\ +f|^t_{\delta h/2,-\delta h,-\delta h} - f|^t_{-\delta h/2,\delta h,\delta h} - f|^t_{-\delta h/2,\delta h,-\delta h} \\ -f|^t_{-\delta h/2,-\delta h,\delta h} - f|^t_{-\delta h/2,-\delta h,-\delta h} \end{pmatrix}, \tag{3}$$

$$\boldsymbol{d}^{(3)}_{u,\delta h}[f] = \frac{1}{4}\begin{pmatrix} f|^t_{\delta h/2,\delta h,0} + f|^t_{\delta h/2,-\delta h,0} + f|^t_{\delta h/2,0,\delta h} \\ +f|^t_{\delta h/2,0,-\delta h} - f|^t_{-\delta h/2,\delta h,0} - f|^t_{-\delta h/2,-\delta h,0} \\ -f|^t_{-\delta h/2,0,\delta h} - f|^t_{-\delta h/2,0,-\delta h} \end{pmatrix}, \tag{4}$$

in which only the respective stencils toward u, v, w are indicated. Equivalently crucial, also, are the q parameters as they ensure stability and well-posedness. Thus, we derive

$$q_1 = p + s(1-p)/3, \quad q_2 = s(1-p)/3, \tag{5a}$$

$$q_3 = 1 - p - 2s(1-p)/3, \tag{5b}$$

with $s(k)$ and $p(k)$ functions given by

$$s(k) = \frac{pR_A + (1-p)R_B - (\cos k - 1)}{(p-1)(R_A + R_B - 2R_C)},$$
$$p(k) = \frac{\cos k_u \cos k_v - \cos k}{1 + \cos k_u \cos k_v - \cos k_u - \cos k_v},$$

while R coefficients are expressed via the wave number, as

$$R_A = \cos k_u + \cos k_v + \cos k_w - 3,$$
$$R_B = \cos k_u \cos k_v \cos k_w - 1,$$
$$R_C = 0.5(\cos k_u \cos k_v + \cos k_u \cos k_w + \cos k_v \cos k_w - 3).$$

Temporal derivatives in Maxwell's equations are computed by means of the properly rearranged nonstandard formula

$$\boldsymbol{DT}^{nst}[f] = \frac{1}{m_\omega(\delta t)}\left(f|^{t+\delta t/2}_u - f|^{t-\delta t/2}_u\right) - \frac{\delta t^2}{24}\,\partial_t^3 f|^t_u, \tag{6}$$

where ∂_t^3 denotes third-order time differentiation and $m_\omega(\delta t)$ is the respective correction function. For time integration (apart from the leapfrog scheme) the fourth-stage Runge–Kutta integrator, which staggers field variables in space but not in time, is also utilized. Its general form is

$$f|^{n+1}_{i,j,k} = \sum_{m=1}^{M} \frac{(-\delta t C)^m}{m!} \cdot f|^n_{i,j,k}, \tag{7}$$

in which C is the spatial discretization matrix and M the order of the integrator. Among the various operators of (7), the fourth-stage seems to be ideal for our higher-order FDTD technique. It is conditionally stable and is not affected by compact differencing. The above form is proven to be 1.4 times more efficient than the respective leapfrog scheme. This increase in performance is attained at the expense of storage requirements. Therefore, the selection of the appropriate time procedure must be a compromise between different factors.

Another important feature of the higher-order curvilinear FDTD concepts, which can sometimes render their utilization prohibitive, is the inevitably widened spatial stencil in the vicinity of perfectly conducting interfaces and absorbing walls. What is apparent in second-order techniques (like the Yee algorithm) where discontinuities are precisely simulated, is not adequate when dealing with higher-order formulae. The stencil of such forms extends at least two nodes on either side of a specific lattice point at which the unknown quantity is defined. Thus, when we reach these areas, problems arise. To circumvent them, we present a general class of self-adaptive compact operators that ensure the meticulous modeling of complex problems and can be expressed via the relation

$$a_1\partial_u f|^t_u + a_2(\partial_u f|^t_{u+\delta h} + \partial_u f|^t_{u-\delta h}) + a_3\delta h(\partial_u^2 f|^t_{u+\delta h} - \partial_u^2 f|^t_{u-\delta h}) + \cdots = b(f|^t_{u+\delta h/2} - f|^t_{u-\delta h/2})/\delta h,$$

where $a_i\,(i = 1, 2, 3)$ and b are unknown coefficients. Their values for the fourth-order operator are $a_1 = 1$, $a_2 = 1/22$, $a_3 = 0$ and $b = 3(3 - a_2)/8$, with an error $[17\delta h^4/5280]\partial_u^5 f$.

III. Formulation of the Div-Curl Problem

The numerical consistency of Maxwell's equations in curvilinear coordinates depends on the choice of the proper basis on which field quantities are expressed [12]–[14]. An incorrect selection may generate the erroneous Cristoffel symbols. Since the FDTD technique is not an exception to this rule, we will develop a new algorithm for the solution of the curvilinear div-curl problem which is a hyperset of Maxwell's equations. The scheme uses a fully conservative higher-order approach of the covariant and contravariant vector component theory and considers all metric terms.

Let us describe our domain by a general nonorthogonal curvilinear coordinate system (u, v, w), smooth enough so that

any vector $\boldsymbol{F}$ can be decomposed in terms of the contravariant $\boldsymbol{a}^1$, $\boldsymbol{a}^2$, $\boldsymbol{a}^3$ or the covariant $\boldsymbol{a}_1$, $\boldsymbol{a}_2$, $\boldsymbol{a}_3$ linear base system as

$$\boldsymbol{F}=\sum_{i=1}^{3}(\boldsymbol{a}_i\cdot\boldsymbol{F})\,\boldsymbol{a}^i=\sum_{i=1}^{3}f_i\boldsymbol{a}^i=\sum_{i=1}^{3}(\boldsymbol{a}^i\cdot\boldsymbol{F})\boldsymbol{a}_i=\sum_{i=1}^{3}f^i\boldsymbol{a}_i.$$

with superscripts and subscripts denoting the contravariant and covariant components. The metrics of the coordinates g_{ij}, g^{ij} are defined by $g_{ij}=g_{ji}=\boldsymbol{a}_i\cdot\boldsymbol{a}_j$, $g^{ij}=g^{ji}=\boldsymbol{a}^i\cdot\boldsymbol{a}^j$ and $g^{1/2}=\boldsymbol{a}_i\cdot(\boldsymbol{a}_j\times\boldsymbol{a}_k)$ with a cyclic permutation of $i,\ j,\ k$. Hence, the curl of vector $\boldsymbol{F}$ can be computed

$$\nabla\times\boldsymbol{F}=\frac{1}{\sqrt{g}}\left[\left(\frac{\partial f_3}{\partial v}-\frac{\partial f_2}{\partial w}\right)\boldsymbol{a}_1+\left(\frac{\partial f_1}{\partial w}-\frac{\partial f_3}{\partial u}\right)\boldsymbol{a}_2+\left(\frac{\partial f_2}{\partial u}-\frac{\partial f_1}{\partial v}\right)\boldsymbol{a}_3\right]$$

Approximation of the derivatives, yields an accurate higher-order curvilinear curl operator which is then applied to Maxwell's equations. For example, the nonstandard Ampere's law is shown in (8)

$$\begin{bmatrix}e_1\\e_2\\e_3\end{bmatrix}_{pos}^{n+1}=\begin{bmatrix}e_1\\e_2\\e_3\end{bmatrix}_{pos}^{n}-m_\omega(\delta t)\left(\frac{\sigma}{\varepsilon}-\frac{\delta t^2}{24}\frac{\partial^3}{\partial t^3}\right)\begin{bmatrix}e_1\\e_2\\e_3\end{bmatrix}_{pos}^{n+1/2}+\frac{m_\omega(\delta t)}{\varepsilon\sqrt{g}}\begin{bmatrix}g_{11}&g_{12}&g_{13}\\g_{21}&g_{22}&g_{23}\\g_{31}&g_{32}&g_{33}\end{bmatrix}\cdot\begin{bmatrix}\boldsymbol{DS}_v^{nst}[h_3]-\boldsymbol{DS}_w^{nst}[h_2]\\\boldsymbol{DS}_w^{nst}[h_1]-\boldsymbol{DS}_u^{nst}[h_3]\\\boldsymbol{DS}_u^{nst}[h_2]-\boldsymbol{DS}_v^{nst}[h_1]\end{bmatrix}_{pos}^{n+1/2}\tag{8}$$

In this expression, σ are the electric losses and *pos* indicates the positions of $\boldsymbol{E}=[e_1,\ e_2,\ e_3]$ or $\boldsymbol{H}=[h_1,\ h_2,\ h_3]$ unknown covariant components (Fig. 1). By substituting the appropriate metric coefficients in these generalized curl equations we can derive the FDTD formulae in any coordinate system.

Therefore, the curvilinear div-curl problem which searches a vector $\boldsymbol{F}$ that its curl and divergence are known, may now be efficiently treated. By using a Helmholtz-type decomposition, we can compute the desired electric or magnetic field via the projection of the curl onto the space of divergence-free vectors [15]. This is the purpose of the unknown quantities in (8). Finally, for $\zeta^{l,m}=u,\ v,\ w$, the stability criterion becomes

$$\pi c\delta t\le 3\sin^{-1}(0.7)\left[\sum_{l=1}^{3}\sum_{m=1}^{3}g^{lm}/(\delta\zeta^l\delta\zeta^m)\right]^{-1/2}.\tag{9}$$

IV. Derivation of the Novel Curvilinear PMLs

The new FDTD technique is now used for the construction of higher-order (HO) curvilinear PML's. It should be stated, that our algorithm has been applied to all existing curvilinear PML methods [7]–[11] in order to improve their absorption, as we will observed from the numerical results section.

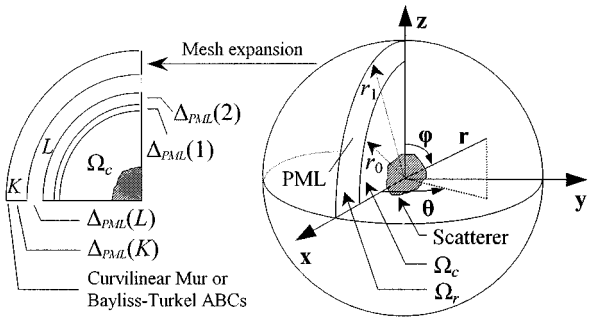

Fig. 3. The geometry of the PML and the mesh expansion procedure.

In the light of their theoretical background, we will investigate the two most complicated formulations. The rest of the techniques are analogously implemented. In the first one, we derive the nonorthogonal version of a 2-D TE split-field absorber. By resolving the magnetic field into two subcomponents, $h_3=h_{3u}+h_{3v}$, the nonstandard FDTD expressions for both the fields in the interior of the layer, which spans between $Luu_{\max}$, can be cast on the form of

$$\varepsilon_0\boldsymbol{DT}^{nst}[h_{3u}]+\sigma h_{3u}=-g^{-1/2}\boldsymbol{DS}_u^{nst}[e_2],\tag{10}$$

$$\varepsilon_0\boldsymbol{DT}^{nst}[h_{3v}]=g^{-1/2}\boldsymbol{DS}_v^{nst}[e_1],\tag{11}$$

$$\varepsilon_0\boldsymbol{DT}^{nst}[e_1]=g^{-1/2}(g_{11}\boldsymbol{DS}_v^{nst}[h_3]-g_{12}\boldsymbol{DS}_u^{nst}[h_3]),\tag{12}$$

$$\varepsilon_0\boldsymbol{DT}^{nst}[e_2]+\sigma e_2=g^{-1/2}(g_{12}\boldsymbol{DS}_v^{nst}[h_3]-g_{22}\boldsymbol{DS}_u^{nst}[h_3]),\tag{13}$$

with $\sigma=\sigma_{\max}[(u-L)/(u_{\max}-L)]^m$ and $m=0,\ 1,\ 2$.

The second case examines the development of a HO unsplit PML in spherical coordinates. The entire space is divided into two parts, as shown in Fig. 3: volume Ω_c which is a sphere of radius r_0 and volume Ω_r extending from r_0 to infinity that must be truncated. The primary goal is to find the proper scaling arguments which will introduce the desired anisotropy in the PML without the need of field splitting. For example, the nonstandard FDTD ϕ-component is given by

$$\boldsymbol{DT}^{nst}[d_\phi]=(\nabla\times\boldsymbol{H})_\phi;$$
$$\boldsymbol{DT}^{nst}[d_\phi]=\varepsilon_0\boldsymbol{DT}^{nst}[e_\phi]+\sigma_r(r)d_\phi,$$

where d_ϕ is the covariant of D_ϕ and $\sigma_r(r)=\sigma_{r,\max}r^m$, $m>0$.

The number of layers can be adequately decreased via a curvilinear mesh expansion technique, according to which the FDTD cell is successively growing in the PML region (Fig. 3). If ξ is the expansion factor then, spatial steps $\Delta_{\rm PML}$ grow as $\Delta_{\rm PML}(L>0)=\xi^L\delta u\ (L=0,\ 1/2,\ 1,\ 3/2,\ \cdots,\ K)$. A carefully selected ξ leads to the suppression of spurious reflections due to the inability of highest frequencies to propagate through the largest cells. Finally, PML's are backed by a lossy version of Bayliss–Turkel (BT) and Engquist–Majda (EM) ABC's, for an additional reduction of lattice errors.

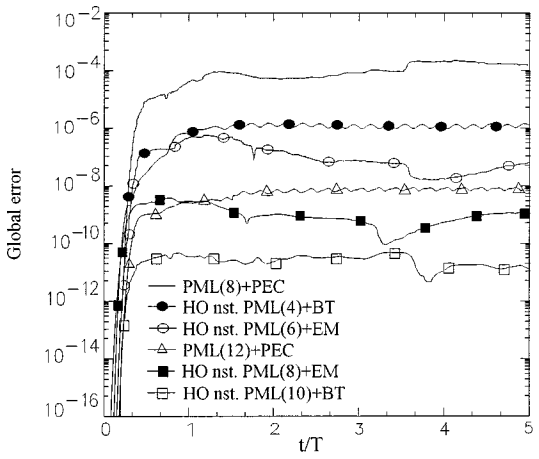

Fig. 4. The variation of global error versus time for various PML schemes.

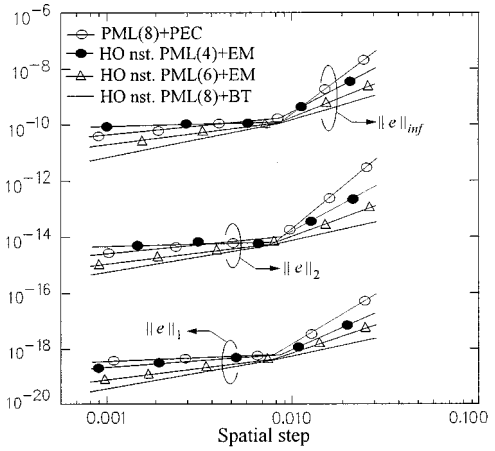

Fig. 5. Convergence of the reflection property for different PML techniques.

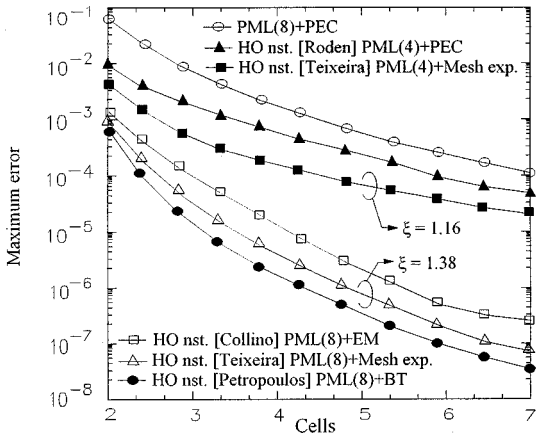

Fig. 6. The variation of maximum error vs. distance from the scatterer.

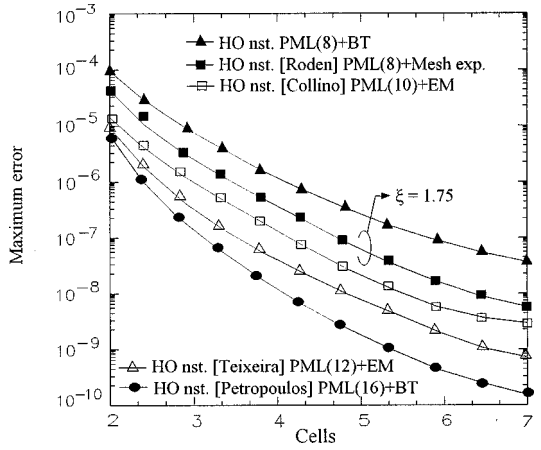

Fig. 7. The behavior of maximum error vs. distance from the scatterer.

V. Conclusions

The absorption of the proposed PML's and all of the curved boundary models are validated via diverse simulations. Since the FDTD method hosts a linear mapping to such problems in respect to memory and CPU requirements, it is apparent that any endeavor regarding grid minimization is of crucial importance as far as efficacy and system resources are concerned. The first problem involves scattering in a 3-D free space. It contains a centered spherical scatterer ($\varepsilon_r = 2.5$) of radius $2cT/3$, illuminated by a magnetic source in $t \in [0, T]$

$$g(t) = \left(10 - 12\cos\frac{2\pi}{T}t + 6\cos\frac{4\pi}{T}t - 4\cos\frac{6\pi}{T}t\right). \tag{14}$$

Reflection errors are computed at the $\theta = \pi/2$ plane. Their definition is the standard one used in the literature (not normalized) and their units are $(\text{A/m})^2$ for the global and A/m for the local error, respectively. We take $T = 1$ nsec. Due to HO schemes, spatial increments are further increased, thus making the mesh variant and very flexible, while the self-adaptive compact operators receive a lossy formulation.

In Fig. 4, the variation of the global error proves that the nonstandard HO PML's outperform their second-order counterparts even with a fairly coarse grid. We also calculate $||e(.)||_l$, for $l = 1, 2, \infty$, on a sequence of grids generated by a successive refinement of their spatial step. Fig. 5 shows the convergence of the reflection property. A promising improvement is achieved by our method combined with the BT or 2nd EM ABC's. Next, the behavior of the existing PML techniques, enhanced by our methodology, is investigated.

In Figs. 6 and 7, the maximum error $e_{\max} = ||e(.)||_{\inf}$ as a function of the distance from the scatterer, is presented. Again, we conclude that the HO PML's exhibit the best performance. Also, the proper value of the expansion factor (as an additional degree of freedom) plays a significant role in the attainment of high attenuation rates and accuracy levels. Finally, an off-centered electric dipole is studied and the evolution of the r-component is shown in Fig. 8. The full absence of nonphysical boundary reflections is evident.

VI. Conclusions

A novel class of accurate higher-order curvilinear PML's based on conventional and nonstandard FDTD concepts, has been presented, in this paper. Self-adaptive compact operators

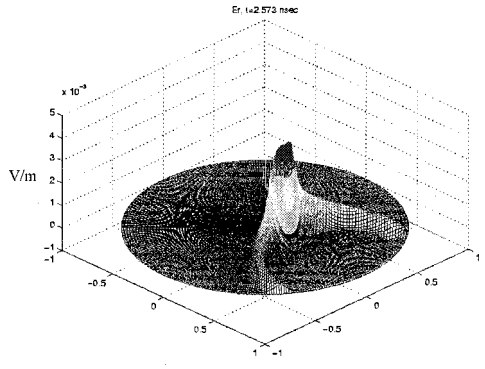

Fig. 8. The evolution of $\boldsymbol{E}$ field r-component via an HO 6-cell PML.

along with general Runge–Kutta integrators are utilized for the efficient treatment of any structural peculiarities. The essential strength of the proposed methodology focuses on their ability to introduce additional attenuation terms along new directions in the medium and the significantly lower dispersion or anisotropy errors. Hence, they require fewer points per wavelength (1/300 that of the Yee algorithm), namely larger spatial cell sizes given a constant error level.

REFERENCES

[1] J.-P. Berenger, *IEEE Trans. Antennas Propagat.*, vol. 45, no. 3, pp. 466–473, Mar. 1997.
[2] W. C. Chew and W. H. Weedon, *Microwave Opt. Technol. Lett.*, vol. 7, no. 13, pp. 599–604, Sept. 1994.
[3] C. M. Rappaport, *IEEE Trans. Magn.*, vol. 32, no. 3, pp. 968–974, May 1996.
[4] L. Zhao and A. C. Cangellaris, *IEEE Microwave Guided Wave Lett.*, vol. 6, no. 5, pp. 209–211, May 1996.
[5] N. Harada and M. Hano, *IEEE Microwave Guided Wave Lett.*, vol. 7, no. 7, pp. 335–337, July 1997.
[6] A. Taflove, Ed., *Advances in Computational Electrodynamics: The Finite-Difference Time-Domain Method*. Boston: Artech House, 1998.
[7] F. L. Teixeira and W. C. Chew, *IEEE Microwave Guided Wave Lett.*, vol. 7, no. 9, pp. 285–287, Sept. 1997.
[8] F. Collino and P. Monk, *SIAM J. Sci. Comp.*, vol. 19, pp. 2061–2090, Sept. 1998.
[9] J. A. Roden and S. D. Gedney, *Microwave Opt. Technol. Lett.*, vol. 14, no. 2, pp. 71–75, 1997.
[10] K.-P. Hwang and J.-M. Jin, *IEEE Microwave Guided Wave Lett.*, vol. 9, no. 4, pp. 137–139, Apr. 1999.
[11] P. G. Petropoulos, SIAM J. Appl. Math., submitted for publication.
[12] J. Fang, "Time Domain Finite Difference Computation for Maxwell's Equations," Ph.D. thesis, Univ. of California, Berkeley, CA, 1989.
[13] J. B. Cole, *IEEE Trans. Microwave Theory Tech.*, vol. 43, no. 9, pp. 2053–2058, Sept. 1995.
[14] R. Schuhmann and T. Weiland, *IEEE Trans. Magn.*, vol. 34, no. 5, pp. 2751–2754, Sept. 1998.
[15] N. V. Kantartzis and T. D. Tsiboukis, *IEEE Trans. Magn.*, vol. 34, no. 5, pp. 2736–2739, Sept. 1998.